JACS
JOURNAL OF THE AMERICAN CHEMICAL SOCIETY

Article

pubs.acs.org/JACS

Single Plasmonic Nanoparticle Tracking Studies of Solid Supported Bilayers with Ganglioside Lipids

Laura B. Sagle,[†] Laura K. Ruvuna,[†] Julia M. Bingham,[§] Chunming Liu,[‡] Paul S. Cremer,[‡] and Richard P. Van Duyne*[,†]

[†]Department of Chemistry, Northwestern University, Evanston, Illinois 60208, United States

[‡]Department of Chemistry, Texas A&M University, College Station, Texas 77843, United States

[§]Department of Chemistry, Saint Xavier University, Chicago, Illinois 60655, United States

Supporting Information

ABSTRACT: Single-particle tracking experiments were carried out with gold nanoparticle-labeled solid supported lipid bilayers (SLBs) containing increasing concentrations of ganglioside (GM_1). The negatively charged nanoparticles electrostatically associate with a small percentage of positively charged lipids (ethyl phosphatidylcholine) in the bilayers. The samples containing no GM_1 show random diffusion in 92% of the particles examined with a diffusion constant of $4.3(\pm4.5) \times 10^{-9}$ cm^2/s. In contrast, samples containing 14% GM_1 showed a mixture of particles displaying both random and confined diffusion, with the majority of particles, 62%, showing confined diffusion. Control experiments support the notion that the nanoparticles are not associating with the GM_1 moieties but instead most likely confined to regions in between the GM_1 clusters. Analysis of the root-mean-squared displacement plots for all of the data reveals decreasing trends in the confined diffusion constant and diameter of the confining region versus increasing GM_1 concentration. In addition, a linearly decreasing trend is observed for the percentage of randomly diffusing particles versus GM_1 concentration, which offers a simple, direct way to measure the percolation threshold for this system, which has not previously been measured. The percolation threshold is found to be 22% GM_1 and the confining diameter at the percolation threshold only ~50 nm.

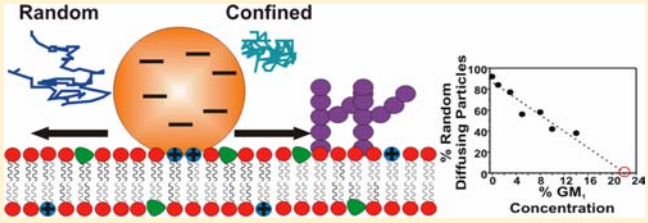

INTRODUCTION

Single-particle tracking experiments utilizing plasmonic nanoparticles have gained popularity in recent years for studying biological phenomena ranging from the motion of motor proteins to membrane fusion in live cells.[1,2] Unlike fluorescence dyes, plasmonic nanoparticles have large scattering cross sections and do not photobleach or blink, which allows for measurements over long time periods.[3] Single-particle tracking has proven particularly useful for studying cellular membranes, since it enables direct characterization of the type of motion of different components in the membrane.[4,5] For example, single-particle tracking of lipids in cellular membranes have greatly increased our understanding of the steps involved in membrane fusion as well as lipid−cytoskeleton interactions.[6,7] In addition, single-particle tracking has been used to study protein−protein interactions in membrane environments.[8] These measurements have allowed for a better understanding of the compartmentalization of proteins in the cell membrane.[9,10]

One of the more prominent ganglioside lipids present in the plasma membranes of mammalian cells, GM_1 is a receptor for both cholera toxin and *Escherichia coli* heat-labile enterotoxin.[11,12] The binding of cholera toxin involves all five B subunits of the protein binding GM_1 and has been extensively studied as a multivalent binding system in cellular membranes.[13−15] Interestingly, unlike other multivalent binding systems in which an increase in binding strength is observed (the K_d value is smaller) with an increase in ligand concentration,[16] the cholera toxin−GM_1 system shows the opposite effect. Mainly, the binding of cholera toxin actually decreases with increasing GM_1 concentration.[17,18] A systematic study of cholera toxin binding to GM_1 was recently carried out using solid supported lipid bilayers (SLBs), a cell membrane mimetic.[19] A model was introduced in which the higher GM_1 concentrations induce clustering of the gangliosides in the bilayer. This clustering of GM_1 within the SLBs is believed to inhibit the binding of cholera toxin. Additional studies using AFM and fluorescence imaging also lend substantial weight to the idea of GM_1 clustering.[20−23]

In addition to the recruitment of bacterial and viral toxins, GM_1 has also been implicated as one of the key components present in lipid rafts domains of cellular membranes, which have a profound influence on cell signaling and trafficking.[24−26] Clusters rich in GM_1 that form in membranes are often modeled as liquid ordered phases, with substantially reduced mobility of their constituent lipids.[27] In addition, the clusters

Received: June 4, 2012
Published: August 31, 2012

   dx.doi.org/10.1021/ja3054095 | J. Am. Chem. Soc. 2012, 134, 15832−15839

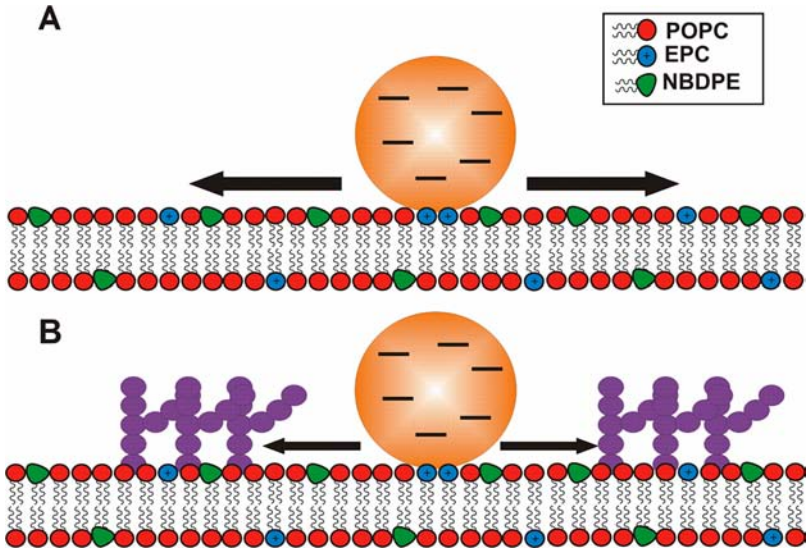

Figure 1. Schematic of how nanoparticle movement changes in bilayers composed of no GM_1 lipids (A) vs bilayers containing >5% GM_1 lipids (B). Nanoparticles electrostatically bound to bilayers containing >5% GM_1 display confined motion that is restricted to the distance between GM_1 clusters. The bilayers are composed of phosphocholine (POPC), ethyl phosphatidylcholine (EPC), nitrobenzoxadiazole phosphoserine (NBDPE), and ganglioside (GM_1). For simplicity, GM_1 molecules in the lower leaflet are not drawn.

promote lipid segregation, with little exchange of lipids between phases.[28] Thus, increasing the GM_1 concentration in a membrane will eventually lead to a percolation threshold, in which the GM_1 clusters are the major component and the fluid phase becomes discontinuous. This has a significant effect on the cell's ability to interact and respond to its environment, since protein components in the fluid part of the membrane are then isolated from each other. Phase behavior of many different types of mixed lipid bilayer systems, such as the liquid/gel phase DMPC/DSPC,[29] liquid/solid phase DPPC/LigGalCer,[30] and DMPC/cholesterol[31,32] have been carried out using techniques such as NMR, ESR, and DSC. Recently, fluorescence recovery after photobleaching (FRAP) has been used to study the connectivity of different components in a mixed lipid bilayer and provided a measurement of the percolation threshold of these systems.[33,34] Unfortunately, trends observed using FRAP are often a result of many underlying mechanisms and further modeling is often required to understand the percolation behavior of the system. Alternatively, a more direct way of measuring a percolation threshold in a mixed lipid system is to carry out single-particle tracking studies, in which the molecule being tracked is only soluble in one component of the mixture.

Herein, we revisit fundamental questions concerning the percolation threshold in mixed lipid bilayers containing increasing concentrations of GM_1 using a single nanoparticle tracking system which can simultaneously measure the position of the nanoparticle (with ±7 nm precision) as well as the plasmonic spectrum. To our knowledge, a fundamental study of percolation and phase behavior of bilayers containing GM_1 using single-particle tracking has not been carried out. The SLBs used here are composed of 0.1% ethyl phosphatidylcholine (EPC), a positively charged lipid that attracts the negatively charged citrate-capped gold nanoparticles. Since particle tracking experiments are able to characterize the type of motion present, it was expected that GM_1 clustering would produce differences in the observed diffusion of these positively charged lipids. In agreement with the GM_1 clustering model, most of the particles observed in the SLBs containing more than 5% GM_1 showed confined motion, in stark contrast to the particles examined in SLBs with no GM_1. As depicted in Figure 1, the data presented herein indicate that the motion of the lipids in bilayers containing >5% GM_1 is confined by the GM_1 clusters themselves. A plot of percent confined particles vs GM_1 concentration shows a linear trend and offers a direct measurement of percolation threshold. This percolation threshold is defined as the GM_1 concentration needed to have 100% confined particles. A plot of percent confined particles vs GM_1 concentration shows this value at 22%. In addition, a linear trend in the diameter of the confining region vs GM_1 concentration yields a diameter of only 50 nm at the percolation threshold, which is 2−5 times the size of a typical membrane protein. Lastly, a decreasing trend observed for the diffusion constants of the confined particles with increasing GM_1 concentration agrees with the notion that diffusion decreases at barriers to the GM_1 clusters.

EXPERIMENTAL METHODS

Small Unilamellar Vesicles and Gold Nanoparticle-Labeled Solid Supported Bilayers. Small unilamellar vesicles (SUVs) were made from 1-palmitoyl-2-oleoyl-*sn*-glycero-3-phosphocholine (POPC), 1-palmitoyl-2-(12-[(7-nitro-2-1,3-benzoxadiazol-4-yl)-amino]dodecanoyl)-*sn*-glycero-3-phosphocholine (NBDPE), and 1,2-dipalmitoyl-*sn*-glycero-3-ethylphosphocholine (EPC), which were all purchased from Avanti Polar Lipids (Alabaster, AL), and ganglioside GM_1, which was purchased from Matreya LLC (Gap, PA). SUVs were prepared by vesicle extrusion, which has been described in detail elsewhere.[35,36] Briefly, this process involved the evaporation of a lipid-chloroform solution under a stream of nitrogen followed by vacuum desiccation for 4 h. The lipids were then rehydrated in phosphate buffered saline (PBS) solution, which consisted of 10 mM sodium phosphate, 150 mM NaCl, and 0.2 mM sodium azide. The pH of the PBS solution was adjusted to 7.4 with small amounts of 1 M HCl. The total concentration of the lipids in solution was 1.0 mg/mL. After several freeze−thaw cycles, the solutions were extruded through a polycarbonate filter (Whatman) with 100 nm pores. The size of the resulting SUVs was confirmed to be 70−80 nm by dynamic light scattering using a Brookhaven Instruments 90Plus particle size analyzer.

dx.doi.org/10.1021/ja3054095 | J. Am. Chem. Soc. 2012, 134, 15832−15839

Solid supported bilayers (SLBs) were formed by incubating the 1.0 mg/mL lipid vesicle solution on glass coverslips (Corning, NY, 22 × 22 mm, No. 2), which were cleaned with boiling 7× detergent and incubated at 500 °C for 5 h. Bilayer formation was assumed to be complete after 10 min incubations at room temperature. The SLBs were washed with copious amounts of deionized (DI) water to remove vesicles not associated with the glass coverslip. The SLBs were then incubated with a solution of 100 nm citrate-capped gold colloids (Ted Pella No. 157113) that was diluted 10× for ca. 1 h. The gold-labeled SLBs were then washed with DI water to remove non-associated nanoparticles.

Fluorescence Recovery after Photobleaching. Confirmation of SLB formation was carried out using FRAP. FRAP experiments were done with a 2.5 W mixed gas argon/krypton ion laser (Stabilite 2018, Spectra Physics). Lipid bilayers were irradiated at 488 nm with 100 mW of power for 2 s. A bleach spot was made on the bilayer using a 10× objective, and fluorescence recovery of the bleached spots was measured as a function of time. The mobile fraction and the half-time of recovery $t_{1/2}$ of NBDPE lipids were determined from single exponential fitting of fluorescence recovery curves. The lateral diffusion coefficient of NBDPE lipids is calculated as follows:[37]

$$D = \frac{w^2}{4t_{1/2}}\gamma_D \quad (1)$$

where w is the radius of the circle disk profile of the bleaching light, and γ_D is a correction factor that depends on the bleach time and the geometry of the laser beam. The value of γ_D and w used were 1.2 and 17.7 μm, respectively. Fitting the data shown in Figure S2a (Supporting Information) for bilayers containing no GM_1 resulted in a diffusion coefficient of 2.5×10^{-8} cm^2/s and 100% mobile fraction. Fitting of the data shown in Figure S2b for bilayers containing 8% GM_1 yielded a diffusion coefficient of 1.9×10^{-8} cm^2/s and 91% mobile fraction.

Single-Particle Tracking. As shown in Figure 2, single-particle tracking experiments were carried out with an inverted microscope (Nikon, Eclipse T*i*-U) equipped with a dark-field condenser (Nikon, NA = 0.8–0.95) and a 100× variable-aperture oil immersion objective (Nikon, NA 0.5–1.3) which was set to NA = 0.5 to collect only the scattered light from the gold nanoparticles. The scattered light from all the nanoparticles in the field of view (80 × 80 μm) was collected and sent through an acoustic-optical tunable filter (Gooch and Housego, His-300 hyperspectral imaging system) which has continuously tunable transmission from 500 to 800 nm and a spectral bandwidth of 1–6 nm. The scattered light was then directed into an EM-CCD camera (Princeton Instruments, proEM512), and the images were stored and analyzed using the LightView (Princeton Instruments) and Matlab (Mathworks, Inc.) software. This allows for one to not only track moving particles with time, but also for the simultaneous collection of the visible spectra. The bandwidth for these experiments was set to 3 nm, and the time resolution of the measurements, 62 ms, was determined by the shutter of the EM-CCD camera plus the readout time. The spatial resolution was determined by approximating the point spread function of a still particle as a two-dimensional Gaussian function and measuring the standard deviation in the centroid of the Gaussian over 300 frames of data (see Figure S3).[38] Briefly, a linescan of a still particle in the x direction was fit to a Gaussian function at each frame. The variance for the centroid of the Gaussian was then calculated for all 300 frames of data. Likewise, a linescan of the same particle in the y direction was fit to a Gaussian function at each frame and the variance calculated for the centroid over 300 frames. The variance in two dimensions was then calculated according to

$$\sigma_{xy} = \sigma_x\sigma_y/\sigma_x + \sigma_y \quad (2)$$

and the standard deviation associated with determining the center of the two-dimensional Gaussian, which determines the spatial resolution, was taken as the square root of the variance. The measured spatial resolution was found to be 6.7 nm. Single nanoparticle trajectories were obtained by marking the x–y centroid position of each particle at each intensity image over time using Matlab.

As noted above, instrumentation recently developed in our laboratory allows for the measurements involved to not only track particles in real time but also acquire a visible spectrum of each particle.[39] The gold nanoparticles used herein contain plasmon resonances in the visible region, which are very sensitive to the local index of refraction.[40,41] Thus, tracking both the LSPR spectral features and motion of the nanoparticles should allow for complex biological interactions to be discerned. To obtain LSPR spectra, the intensities collected for the nanoparticles in the field of view from 500 to 800 nm was divided by a spectrum collected with no sample (dark) and the full lamp intensity over the same wavelength values and time scales in Matlab. Representative LSPR spectra for the gold nanoparticles used are shown in Figures 3 and 4.

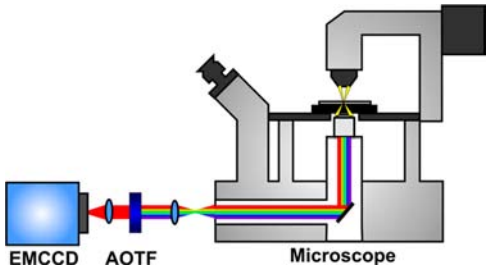

Figure 2. Setup used to carry out single nanoparticle tracking experiments. Samples are mounted on an inverted microscope and viewed through a 100× oil immersion objective. A dark field condenser is placed on top of the sample so that only the scattered light is measured. The scattered light at all wavelengths then passes through the objective, a coupling lens and into a set of acousto-optical tunable filters (AOTF) where only one wavelength of light goes through to the EMCCD camera at a given time. This allows for the simultaneous acquisition of the particles position as well as the scattering spectrum.

RESULTS

Single nanoparticle trajectories were collected in thirty to forty different areas of SLB samples containing no GM_1. Each 80 × 80 μm area contained several moving nanoparticles enabling the acquisition of close to 100 different trajectories. It is important to note that many of the nanoparticles in the field of view (approximately 20–40%) were stationary and it was assumed that these particles were bound to the glass via defects present in the SLBs. Of the particles examined, 92% showed random diffusion, with the other 8% of particles displaying confined diffusion. Due to defects in the bilayer, the small amount of confined diffusion observed here could be the result of particles trapped between two defect sites. The trajectories and mean squared displacement plots of three representative particles is shown in Figure 3. The plots for the particles shown are linear, indicating the diffusion is random, Brownian motion and can be fit to the expression, $\langle r^2\rangle = 4Dt$, where $\langle r^2\rangle$ is the mean-squared displacement, D the diffusion constant, and t the time lag. Fitting the plots shown in Figure 3 with a linear regression yields diffusion constants of 8.0×10^{-9}, 2.8×10^{-9}, and 6.5×10^{-9} cm^2/s for particles 1, 2, and 3, respectively. Taking into account all the particles (at different GM_1 concentrations) that also showed the same linear behavior, an average value of the diffusion constant was found to be $4.3(\pm 4.5) \times 10^{-9}$ cm^2/s. This value is consistent with other literature studies, which used single-particle tracking of 50 nm gold nanoparticles on SLBs and fall within the range of 1×10^{-8}–1×10^{-9} cm^2/s.[42−44] Additionally, Figure 3C shows

dx.doi.org/10.1021/ja3054095 | J. Am. Chem. Soc. 2012, 134, 15832–15839

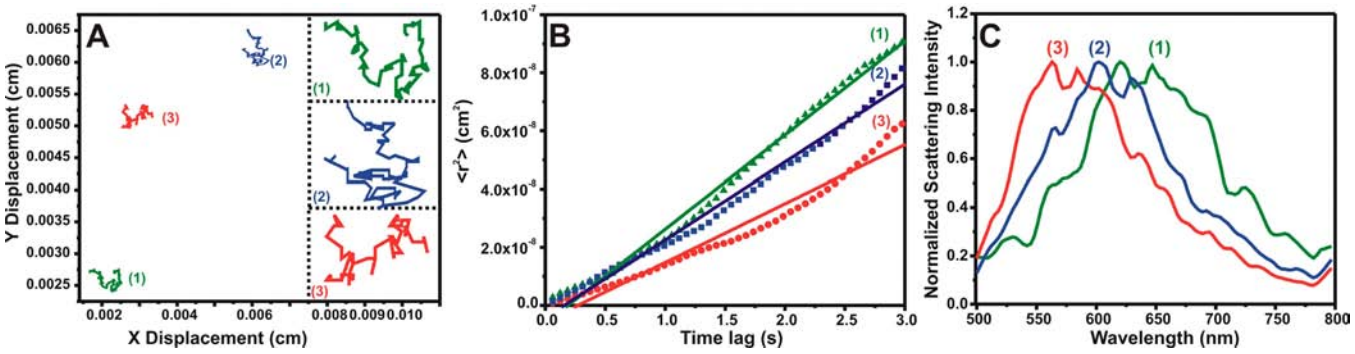

Figure 3. Trajectories of three particles in bilayers without GM_1 (A). Plot of root-mean-squared displacement vs time lag (B) and LSPR spectra (C) for the three particles shown in (A). The LSPR spectra were obtained with the particle trajectories simultaneously by scanning the AOTF from 500 to 800 nm as the particles are moving. The LSPR spectra were further smoothed using a Loess polynomial regression function. The root-mean-squared displacement plots of all three particles show a clear linear trend indicating their motion is Brownian.

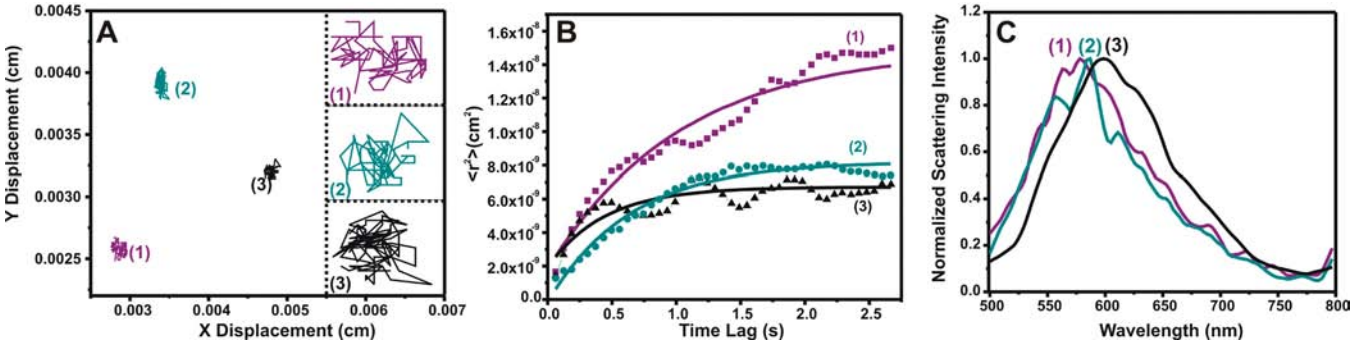

Figure 4. Trajectories of three particles in bilayers with 10% GM_1 (A). Plot of root-mean-squared displacement vs time lag (B) and LSPR spectra (C) for the three particles shown in (A). The dashed line through the points plotted in (B) is the fit to the equation $\langle r^2\rangle = \langle r^2\rangle[1 - A_1 \exp(-4A_2Dt/\langle r_c^2\rangle)]$, which is typically used to describe confined motion. In the above expression, $\langle r_c^2\rangle$ is the asymptotic value where r_c is the radius of the confining region, D is the diffusion constant in cm^2/s, and A_1 and A_2 are factors relating to the geometry of the confining region. The LSPR spectra were further smoothed using a Loess polynomial regression function.

LSPR spectra of corresponding particles whose trajectories are shown in 3a.

Next, gold nanoparticles electrostatically bound to bilayers containing 1%, 3%, 5%, 8%, 10%, and 14% GM_1 were measured. For each concentration of GM_1, more than 40 particle trajectories were analyzed, and a linearly increasing trend in the number of confined particles was observed. However, even with SLBs containing significant concentrations of GM_1, a considerable amount of particles showed Brownian diffusion with diffusion constants similar to what was observed in the samples containing no GM_1. It is assumed that the density of GM_1 throughout the SLB is not uniform and that there were simply no GM_1 clusters in the near vicinity of these randomly diffusing particles. The resulting trajectories and mean squared displacement plots for three particles in SLBs containing 10% GM_1 are shown in Figure 4. As shown in Figure 4B, the raw data are fit to the following expression for confined diffusion:

$$\langle r^2\rangle = \langle r^2\rangle[1 - A_1 \exp(-4A_2Dt/\langle r_c^2\rangle)] \quad (3)$$

where $\langle r_c^2\rangle$ is the square of the confined radius with which the particles themselves are confined (which is the asymptotic value), A_1 and A_2 are geometric factors relating to the shape of the confining region, and D is the diffusion constant for the confined particle.[43] The average diffusion constant and confined diameter obtained from fitting the root-mean-squared displacement plots shown in Figure 4 are 9.5×10^{-9} cm^2/s and 830 nm, respectively. The value of confined diameter measured here, is considerably larger than that obtained for a GM_1 cluster using atomic force microscopy (20−200 nm), and even that which was reported for a lipid raft (100−200 nm).[45,46] Thus, it is reasonable to assume these particles are in fact bound to the positively charged lipids themselves and not the GM_1 moieties.

Nevertheless, several control experiments were carried out to confirm that the particles measured were indeed electrostatically bound to the bilayers, and not associating with the GM_1 moieties. In the first control experiment, images were taken of gold nanoparticles bound to the SLBs containing no GM_1 with and without salt in solution. If the particles are electrostatically bound to the bilayers, this interaction should be screened to some degree by adding salt. Figure S4 does show significantly fewer particles bound to the bilayers in the presence of salt in the solution. The next control experiment investigated the binding of negatively charged nanoparticles to bilayers both with and without positively charged lipid. Figure S5 describes a set of images taken with bilayers varying only in positively charged lipid composition. Although most of the images comparing bilayers with and without positively charged lipid show greater numbers of nanoparticles in the former, it was sometimes observed that a comparable number of charged nanoparticles would reside at the bilayer surface in the sample without positively charged lipids. However, these nanoparticles would quickly go out of the field of view, making particle tracking for 300 frames difficult. Thus, this dissociation from the bilayers containing no positively charged lipid offers

dx.doi.org/10.1021/ja3054095 | J. Am. Chem. Soc. 2012, 134, 15832−15839

Table 1. Measured Diffusion Parameters for Individual Particles

			diffusion constant (cm^2/s)		
GM_1 concn (%)	no. of particles measured	random diffusion (%)	random	confined	confined diameter (nm)
0	95	92	$4.3(\pm4.5) \times 10^{-9}$	$1.3(\pm0.8) \times 10^{-8}$	1300(±1100)
1	63	84	$3.8(\pm3.9) \times 10^{-9}$	$2.0(\pm0.7) \times 10^{-8}$	1100(±1100)
3	81	77	$9.6(\pm5.6) \times 10^{-10}$	$1.1(\pm0.5) \times 10^{-8}$	1500(±410)
5	45	56	$2.9(\pm4.4) \times 10^{-9}$	$7.9(\pm3.9) \times 10^{-9}$	870(±470)
8	51	59	$2.1(\pm4.5) \times 10^{-9}$	$9.6(\pm8.3) \times 10^{-9}$	680(±570)
10	43	42	$2.3(\pm2.8) \times 10^{-9}$	$1.7(\pm1.4) \times 10^{-10}$	820(±500)
14	52	38	$9.4(\pm6.7) \times 10^{-10}$	$1.8(\pm1.8) \times 10^{-10}$	560(±210)

additional proof of this electrostatic interaction between nanoparticles and the bilayer. The third control experiment was performed to look at the localized surface plasmon resonance (LSPR) spectra of the particles in H_2O, bound to SLBs containing no GM_1, and bound to SLBs containing 10% GM_1. The LSPR spectra of these particles are extremely sensitive to the refractive index of the surrounding media and should be a measure of how the particles are associating and interacting with the SLBs. As shown in Figure S6, the maximum in the LSPR spectrum does shift slightly upon binding SLBs, but no further shift is observed when binding to SLBs containing GM_1, also supporting the notion that the particles themselves are not associating with GM_1. Lastly, we wished to confirm that the binding of the nanoparticles to the SLBs is not affected by the size or capping agent of the particles. Thus, single-particle tracking experiments were carried out using 50 nm citrate-capped gold nanoparticles purchased from CABOT (instead of Ted Pella) with SLBs containing 1% GM_1. These data showed diffusion constants for both the confined and randomly diffusing particles to be similar to that observed with the Ted Pella particles, $1.1(\pm1.3) \times 10^{-8}$ and $6.5(\pm6.1) \times 10^{-9}$ cm^2/s, respectively. In addition, the percent randomly diffusing particles, 86%, is also similar to what was observed with the Ted Pella particles.

The parameters obtained from fitting the root-mean-squared displacement plots for all the particles measured in bilayers containing 0%, 1%, 3%, 5%, 8%, 10%, and 14% GM_1 are shown in Table 1. As shown in column 3 of Table 1, the percentage of randomly diffusing particles decreases with GM_1 concentration in a linear fashion. The diffusion constants for the randomly diffusing particles, column 4, show little change with increasing GM_1 in the bilayers. In contrast, diffusion constants for confined particles show a marked decrease with GM_1 concentration. Lastly, the diameter of the confining region for the confined particles also shows a decreasing trend with GM_1 concentration. To further illustrate the trends observed in columns 5 and 6 of Table 1, histogram plots were generated which tallied the diffusion constants and confining diameter for each confined particle at all the GM_1 concentrations measured, Figure 5.

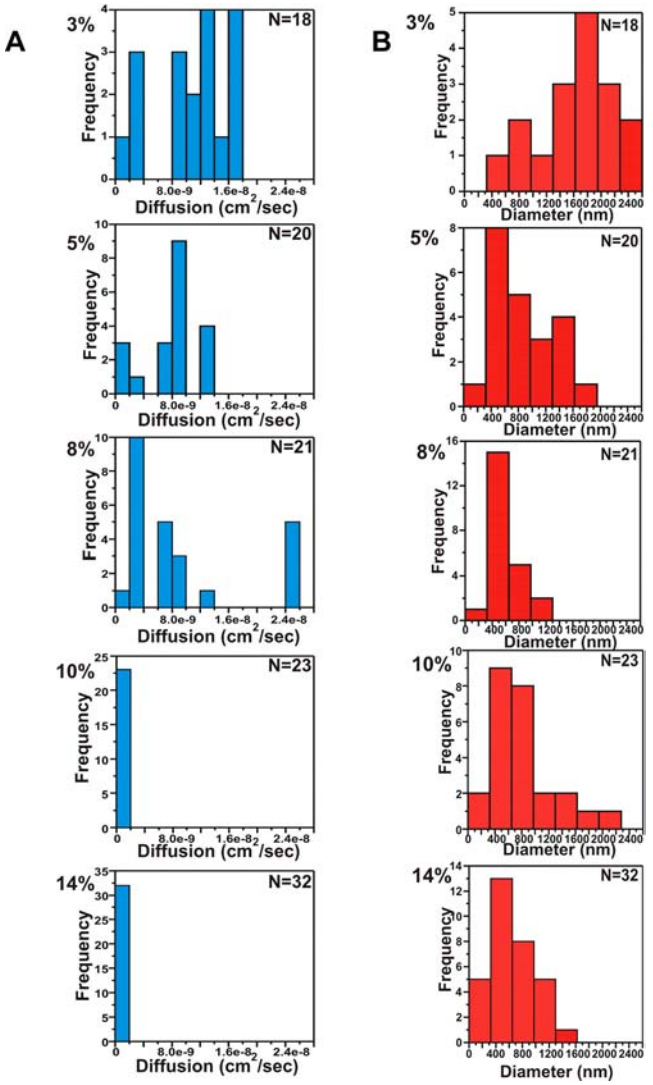

Figure 5. Series of histogram plots showing how the diffusion constant of the confined particles decreases with increasing GM_1 concentration (A). Histogram plots showing a decreasing trend in the confined radius with increasing GM_1 concentration (B). Histogram plots for 0% and 1% GM_1 are not shown since the number of confined particles was small.

DISCUSSION

McConnell and co-workers[47] first established in 1975 that biological membranes consist of many components that can exist in a variety of phases. The connection between the existence of liquid condensed regions in membranes and their possible effects on cellular processes relies on their ability to compartmentalize membrane components through selective permeability and reduced mobility. Indeed, several recent studies involving FRAP, single-particle tracking, and fluorescence correlation spectroscopy show greatly decreased mobility in clustered domains.[48,49] Additionally, selective permeability of lipids and membrane components in and out of raft-like domains has also been studied extensively.[28,50] Our results support a model of GM_1 clustering into domains at concentrations above 5% GM_1. Moreover, the nanoparticles

dx.doi.org/10.1021/ja3054095 | J. Am. Chem. Soc. 2012, 134, 15832−15839

associated with the lipids in the fluid phase are not observed to partition into the GM_1 clusters, indicating selective permeability. Instead, the GM_1 clusters themselves act as barriers to the nanoparticles whose motion is confined to smaller domains of the fluid phase at high concentrations of GM_1. This notion is supported by all the trends shown in Table 1 with increasing GM_1 concentrations; increasing amounts of confined particles, decreasing diameters for the confining regions and a decrease in the diffusion constants of the confined particles.

If the function of a cluster with decreased mobility is to physically compartmentalize the membrane components and control, to some degree, membrane partitioning, the interconnectivity of the condensed and liquid phase is extremely important for cellular function. A parameter that describes the connectivity of two phases that make up a membrane is the percolation threshold. Below the percolation threshold, the fluid phase, making up the majority of the bilayer, is interconnected and consists of small island-like structures of GM1-rich domains (similar to what has previously been observed for metallic films).[51] At and above the percolation threshold, this fluid phase is broken up by the GM_1-rich domains, creating an obstacle to a membrane component soluble in the fluid phase that is attempting to diffuse from one part of the membrane to another. In the simple model membrane systems studied here, anomalous diffusion was observed in less than 1% of the particles examined, and in order to focus on the majority of the particles, these data were excluded from the paper. Therefore, 99% of the particles examined simply showed either random or confined diffusion, making the analysis quite straightforward. It is also important to note that the time scales of the measurements described herein are quite short (only 3 s) and possibly not long enough to observe events involving hopping between adjacent domains. Since the particles are restricted solely to the fluid phase without GM_1, a percolation threshold value is defined as the concentration of GM_1 needed to have 100% confined particles. Thus, if all of the fluid phase particles are confined, the clusters containing GM_1 must be interconnected. Percolation threshold values have been obtained for mixed bilayer systems, typically using FRAP, but these values rely on a knowledge of the geometry of the confining region as well as the geometry of the bleach spot.[29,52,53] Our value of percolation threshold does not rely on *a priori* knowledge of the growth of the confining regions and their geometry and is therefore a more direct measurement. The value for percolation threshold for this system is simply obtained from plotting the % randomly diffusing particles versus GM_1 concentration. As shown in Figure 6, this plot shows a linear trend and through linear extrapolation, a percolation threshold value of 22% is obtained. This value is similar to what has been observed using FRAP with mixed bilayer systems containing liquid and gel phase lipids, such as DLPC/DSPC and DMPC/DSPC, which are also believed to segregate into domains.[29] The percolation threshold value of 22% GM_1 is higher than that observed in biological cells, with a value of 10−12% GM_1 observed in neurons being the highest.[54] However, it should be noted that the GM_1 moieties are most likely asymmetrically distributed among the two leaflets of the membrane giving rise to higher concentrations on the outer surface of the cell.[55] It should also be noted that there is a growing number of studies that show using charged probe molecules can affect the distribution and mobility of lipids within the bilayer.[49,56,57] In addition, cells contain other ganglioside components, such as GM_2, GM_3, and GD_3, that would most likely co-cluster with GM_1 creating larger clusters from smaller concentrations of GM_1.[11,58] This somewhat low percolation threshold value is often associated with the solid-like and fluid-like domains being asymmetric.[59,60] The value for percolation threshold obtained herein describes the amount of GM_1 required to inhibit the movement of a membrane component confined to the mobile phase.

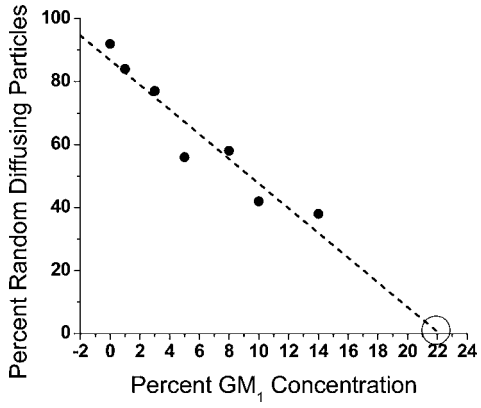

Figure 6. Plot of percent confined particles vs GM_1 concentration, showing a linear trend. It is expected that at the percolation threshold, 100% of the particles would show confined behavior, thus the percolation threshold is defined as the GM_1 concentration at 0% randomly diffusing particles. Linear extrapolation (dashed line) through the points reveals a percolation threshold value of 22% GM_1.

Another interesting question addresses the size of these confining regions at the percolation threshold that perhaps contain membrane proteins vital for cellular function. Single-particle tracking measurements allow for a direct measurement of the confined diameter for each confined particle through the asymptotic value in the root-mean-squared displacement plot. As expected, the confined diameter for the particles in the fluid phase is reduced as more GM_1 are added to the bilayer, increasing the surface area of the solid phase. A plot of the average confined diameter for the particles versus GM_1 concentration shows a steeply descending linear trend (see Figure 7). Extrapolation of this line to the percolation threshold value yields a confined diameter of only 50 nm. Given the large error in measuring this value on a per particle basis, the value of the confined diameter at the percolation threshold most likely

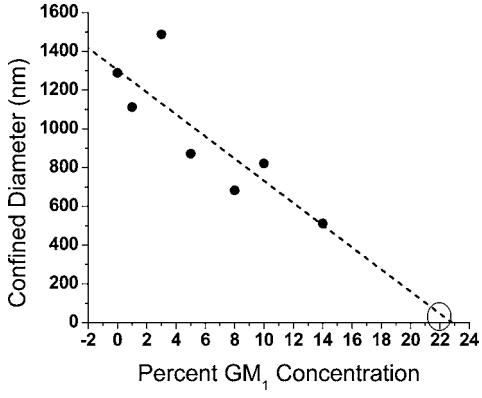

Figure 7. Plot of confined diameter for the particles exhibiting confined behavior vs GM_1 concentration, showing a linear trend. Linear extrapolation (dashed line) through the points reveals a confined diameter of only 50 nm at the percolation threshold.

dx.doi.org/10.1021/ja3054095 | J. Am. Chem. Soc. 2012, 134, 15832−15839

varies between 0 and 200 nm. Even so, this value is the same order of magnitude of membrane protein complexes and indicates a surprisingly restricted fluid phase.

The last trend of interest shown in Table 1 is the diffusion constant values for confined particles decreases with increasing GM_1 concentrations. This trend is further illustrated in Figure 5A, where the histograms center around smaller values at higher GM_1 concentrations. Saxton et al. have calculated that lateral diffusion in the fluid phase should slow down in a linear fashion as more solid obstacles are added.[61] Interestingly, a linearly decreasing trend is observed here, but only for the confined particles. The randomly diffusing particles, even at high concentrations of GM_1, still show diffusion constants similar to those with no GM_1 present, possibly indicating that the GM_1 clusters are not evenly dispersed throughout the bilayers. This notion is also supported by the possibility of an asymmetric distribution of domains suggested by the low percolation threshold value. In addition, AFM and fluorescence microscopy measurements of GM_1 domains in phosphtidylcholine bilayers made through vesicle fusion also support this idea.[23] The linearly decreasing trend in diffusion coefficients with increasing concentrations of an immiscible phase has been observed previously when the two phases have drastically different mobilites.[62] Thus, the linear trend observed is in agreement with the notion that the GM_1 clusters have substantially reduced mobility. This is also in agreement with single molecule measurements showing that the lipid molecules within GM_1 clusters are significantly less mobile.[63] For particles confined in the fluid phase, as the GM_1 concentration is increased, larger amounts of immobile clusters appear, which take up a larger percentage of surface area. In turn, the fluid phase contains a smaller surface area, with each confined particle surrounded by an increased solid phase boundary. The slowed diffusion measured for particles in smaller confined regions is in agreement with both experimental and theoretical results, and supports the existence of a boundary layer around the solid-like obstacles.[33,64,65] Thus, the data indicate that the GM_1 clusters most likely contain boundary regions in contact with the fluid phase where diffusion is considerably slower.

CONCLUSIONS

This study reports single-particle tracking experiments for gold nanoparticle-labeled SLBs containing increasing concentrations of GM_1. The SLBs used in this paper are a model system for a cellular membrane containing many different components whose communication relies, to a large degree, on membrane fluidity. Upon addition of increasing amounts of GM_1 to the SLBs, higher percentages of particles showed confined diffusion. Since it has been shown that GM_1 clusters exist in SLBs containing greater than 5% GM_1, our data indicate that these particles are most likely confined to the regions between GM_1 clusters. Values for the diffusion constants for both random and confined particles as well as an estimate of the radius of the confined region are obtained from root-mean-squared displacement plots. The data show that although the diffusion constants for the randomly diffusing particles does not significantly change upon addition of GM_1, both the diffusion constants and the confined radius markedly decrease with GM_1 concentration for the confined particles. One question of biological importance is the concentration of GM_1 needed to produce a bilayer in which the fluid phase is no longer interconnected, resulting in confined behavior for all of its constituents, and is referred to as the percolation threshold. A plot of the percent of randomly diffusing particles versus GM_1 concentration shows a simple linear trend, which when extrapolated to 0% randomly diffusing particles gives a percolation threshold value of 22% GM_1. When a plot of confined diameter versus GM_1 concentration is extrapolated to the value of 22%, it is revealed that the confined diameter of the fluid phase at the percolation threshold is only ~50 nm. Thus, at the percolation threshold, membrane components in the fluid phase are drastically confined to regions that are the same order of magnitude as the membrane proteins themselves.

This single-particle tracking study can be expanded to further explore membrane fluidity and binding interactions using SLBs in which the motion of the nanoparticle and its LPSR spectrum can be simultaneously monitored. In addition, aggregation of peripheral membrane components in real time can be studied through both their diffusion trajectories and LSPR spectral features.

ASSOCIATED CONTENT

Supporting Information

Details on FRAP measurements and various control experiments described in the Results section. This material is available free of charge via the Internet at http://pubs.acs.org.

AUTHOR INFORMATION

Corresponding Author

vanduyne@northwestern.edu

Notes

The authors declare no competing financial interest.

ACKNOWLEDGMENTS

R.P.V.D. thanks the National Science Foundation (EEC-0647560, CHE-1025947, HDTRA1-09-1-0007), and P.S.C. thanks the National Institutes of Health (GM070622) for funding.

REFERENCES

(1) Cai, D.; Verhey, K. J.; Meyhofer, E. *Biophys. J.* **2007**, 201a–202a.
(2) Floyd, D. L.; Ragains, J. R.; Skehel, J. J.; Harrison, S. C.; van Oijen, A. M. *Proc. Natl. Acad. Sci. U.S.A.* **2008**, *105*, 15382–15387.
(3) Nallathamby, P. D.; Lee, K. J.; Xu, X. H. N. *ACS Nano* **2008**, *2*, 1371–1380.
(4) Saxton, M. J.; Jacobson, K. *Annu. Rev. Biophys. Biomol. Struct.* **1997**, *26*, 373–399.
(5) Garcia-Saez, A. J.; Schwille, P. *Biochim. Biophys. Acta-Biomembranes* **2010**, *1798*, 766–776.
(6) Wessels, L.; Elting, M. W.; Scimeca, D.; Weninger, K. *Biophys. J.* **2007**, *93*, 526–538.
(7) Brown, F. L. H.; Leitner, D. M.; McCammon, J. A.; Wilson, K. R. *Biophys. J.* **2000**, *78*, 2257–2269.
(8) Fujiwara, T.; Ritchie, K.; Murakoshi, H.; Jacobson, K.; Kusumi, A. *J. Cell Biol.* **2002**, *157*, 1071–1081.
(9) Simson, R.; Sheets, E. D.; Jacobson, K. *Biophys. J.* **1995**, *69*, 989–993.
(10) Day, C. A.; Kenworthy, A. K. *Biochim. Biophys. Acta-Biomembranes* **2009**, *1788*, 245–253.
(11) Mocchetti, I. *Cell. Mol. Life Sci.* **2005**, *62*, 2283–2294.
(12) Chen, J. C.; Chang, Y. S.; Wu, S. L.; Chao, D. C.; Chang, C. S.; Li, C. C.; Ho, T. Y.; Hsiang, C. Y. *J. Ethnopharmacol.* **2007**, *113*, 233–239.
(13) Holmgren, J.; Lonnroth, I.; Mansson, J. E.; Svennerholm, L. *Proc. Natl. Acad. Sci. U.S.A.* **1975**, *72*, 2520–2524.
(14) Merritt, E. A.; Sarfaty, S.; Vandenakker, F.; Lhoir, C.; Martial, J. A.; Hol, W. G. J. *Protein Sci.* **1994**, *3*, 166–175.

(15) Blank, N.; Schiller, M.; Krienke, S.; Wabnitz, G.; Ho, A. D.; Lorenz, H. M. *Immunol. Cell Biol.* **2007**, *85*, 378−382.
(16) Yang, T. L.; Baryshnikova, O. K.; Mao, H. B.; Holden, M. A.; Cremer, P. S. *J. Am. Chem. Soc.* **2003**, *125*, 4779−4784.
(17) MacKenzie, C. R.; Hirama, T.; Lee, K. K.; Altman, E.; Young, N. M. *J. Biol. Chem.* **1997**, *272*, 5533−5538.
(18) Lencer, W. I.; Chu, S. H. W.; Walker, W. A. *Infect. Immun.* **1987**, *55*, 3126−3130.
(19) Shi, J. J.; Yang, T. L.; Kataoka, S.; Zhang, Y. J.; Diaz, A. J.; Cremer, P. S. *J. Am. Chem. Soc.* **2007**, *129*, 5954−5961.
(20) Reed, R. A.; Shipley, G. G. *Biophys. J.* **1996**, *70*, 1363−1372.
(21) Thompson, T. E.; Allietta, M.; Brown, R. E.; Johnson, M. L.; Tillack, T. W. *Biochim. Biophys. Acta* **1985**, *817*, 229−237.
(22) Wang, R.; Shi, J.; Parikh, A. N.; Shreve, A. P.; Chen, L. H.; Swanson, B. I. *Colloids Surf. B-Biointerfaces* **2004**, *33*, 45−51.
(23) Yuan, C. B.; Johnston, L. J. *Biophys. J.* **2001**, *81*, 1059−1069.
(24) Korade, Z.; Kenworthy, A. K. *Neuropharmacology* **2008**, *55*, 1265−1273.
(25) Pike, L. J. *J. Lipid Res.* **2009**, *50*, S323−S328.
(26) Simons, K.; Ikonen, E. *Nature* **1997**, *387*, 569−572.
(27) Kaiser, H. J.; Lingwood, D.; Levental, I.; Sampaio, J. L.; Kalvodova, L.; Rajendran, L.; Simons, K. *Proc. Natl. Acad. Sci. U.S.A.* **2009**, *106*, 16645−16650.
(28) Kahya, N.; Scherfeld, D.; Bacia, K.; Poolman, B.; Schwille, P. *J. Biol. Chem.* **2003**, *278*, 28109−28115.
(29) Vaz, W. L. C.; Melo, E. C. C.; Thompson, T. E. *Biophys. J.* **1989**, *56*, 869−876.
(30) Almeida, P. F. F.; Vaz, W. L. C.; Thompson, T. E. *Biochemistry* **1992**, *31*, 7198−7210.
(31) Vist, M. R.; Davis, J. H. *Biochemistry* **1990**, *29*, 451−464.
(32) Sankaram, M. B.; Thompson, T. E. *Proc. Natl. Acad. Sci. U.S.A.* **1991**, *88*, 8686−8690.
(33) Almeida, P. F. F.; Vaz, W. L. C.; Thompson, T. E. *Biochemistry* **1992**, *31*, 6739−6747.
(34) Vaz, W. L. C.; Almeida, P. F. F. *Curr. Opin. Struct. Biol.* **1993**, *3*, 482−488.
(35) Brian, A. A.; Mcconnell, H. M. *Proc. Natl. Acad. Sci. U.S.A.-Biol. Sci.* **1984**, *81*, 6159−6163.
(36) Cremer, P. S.; Groves, J. T.; Kung, L. A.; Boxer, S. G. *Langmuir* **1999**, *15*, 3893−3896.
(37) Axelrod, D.; Koppel, D. E.; Schlessinger, J.; Elson, E.; Webb, W. W. *Biophys. J.* **1976**, *16*, 1055−1069.
(38) Yildiz, A.; Forkey, J. N.; McKinney, S. A.; Ha, T.; Goldman, Y. E.; Selvin, P. R. *Science* **2003**, *300*, 2061−2065.
(39) Bingham, J. M.; Willets, K. A.; Shah, N. C.; Andrews, D. Q.; Van Duyne, R. P. *J. Phys. Chem. C* **2009**, *113*, 16839−16842.
(40) Willets, K. A.; Van Duyne, R. P. *Annu. Rev. Phys. Chem.* **2007**, *58*, 267−297.
(41) Sagle, L. B.; Ruvuna, L. K.; Ruemmele, J. A.; Van Duyne, R. P. *Nanomedicine* **2011**, *6*, 1447−1462.
(42) Lee, G. M.; Ishihara, A.; Jacobson, K. A. *Proc. Natl. Acad. Sci. U.S.A.* **1991**, *88*, 6274−6278.
(43) Sheets, E. D.; Lee, G. M.; Simson, R.; Jacobson, K. *Biochemistry* **1997**, *36*, 12449−12458.
(44) Pinaud, F.; Michalet, X.; Iyer, G.; Margeat, E.; Moore, H. P.; Weiss, S. *Traffic* **2009**, *10*, 691−712.
(45) Coban, O.; Burger, M.; Laliberte, M.; Ianoul, A.; Johnston, L. J. *Langmuir* **2007**, *23*, 6704−6711.
(46) Hancock, J. F. *Nat. Rev. Mol. Cell Biol.* **2006**, *7*, 456−462.
(47) Wu, S. H. W.; Mcconnell, H. M. *Biochemistry* **1975**, *14*, 847−854.
(48) Simons, K.; Vaz, W. L. C. *Annu. Rev. Biophys. Biomol. Struct.* **2004**, *33*, 269−295.
(49) Burns, A. R.; Frankel, D. J.; Buranda, T. *Biophys. J.* **2005**, *89*, 1081−1093.
(50) Rietveld, A.; Simons, K. *Biochim. Biophys. Acta-Rev. Biomembranes* **1998**, *1376*, 467−479.
(51) Morris, J. E.; Coutts, T. J. *Thin Solid Films* **1977**, *47*, 3−65.
(52) Bar, L. K.; Barenholz, Y.; Thompson, T. E. *Biochemistry* **1997**, *36*, 2507−2516.
(53) Schram, V.; Lin, H. N.; Thompson, T. E. *Biophys. J.* **1996**, *71*, 1811−1822.
(54) Saqr, H. E.; Omran, O.; Dasgupta, S.; Yu, R. K.; Oblinger, J. L.; Yates, A. J. *J. Neurochem.* **2006**, *96*, 1301−1314.
(55) Shreve, A. P.; Howland, M. C.; Sapuri-Butti, A. R.; Allen, T. W.; Parikh, A. N. *Langmuir* **2008**, *24*, 13250−13253.
(56) Kasbauer, M.; Junglas, M.; Bayerl, T. M. *Biophys. J.* **1999**, *76*, 2600−2605.
(57) Klymchenko, A. S.; Duportail, G.; Demchenko, A. P.; Mely, Y. *Biophys. J.* **2004**, *86*, 2929−2941.
(58) Livingston, P. O.; Ritter, G.; Calves, M. J. *Cancer Immunol. Immun.* **1989**, *29*, 179−184.
(59) Xia, W.; Thorpe, M. F. *Phys. Rev. A* **1988**, *38*, 2650−2656.
(60) Garboczi, E. J.; Thorpe, M. F.; Devries, M. S.; Day, A. R. *Phys. Rev. A* **1991**, *43*, 6473−6482.
(61) Saxton, M. J. *Biophys. J.* **1982**, *39*, 165−173.
(62) Saxton, M. J. *Biophys. J.* **1987**, *52*, 989−997.
(63) Lagerholm, B. C.; Weinreb, G. E.; Jacobson, K.; Thompson, N. L. *Annu. Rev. Phys. Chem.* **2005**, *56*, 309−336.
(64) Saxton, M. J. *Biophys. J.* **1989**, *56*, 615−622.
(65) Blackwell, M. F.; Whitmarsh, J. *Biophys. J.* **1990**, *58*, 1259−1271.